

Damage Resistance Characteristics of Thick-Core Honeycomb Composite Panels

Paolo Feraboli¹

University of Washington, Seattle, WA 98195-2400

The quasi-static indentation and impact response of very thick sandwich panels, developed as candidate materials for the crown panel of the next generation large commercial transport, is described. A preliminary characterization of the damage resistance of eight different core-facesheet configurations is performed, and the effect of facesheet thickness, core density and core material is investigated. Drop weight impact, quasi-static indentation, and quasi-static core-crushing characteristics of the different core panel configurations have been studied. Damage is evaluated using conventional methods including cross-sectioning and visual inspection, and dent depth is measured by means of an automated high-precision depth gage. The indentation profile is monitored by means of the digital image correlation technique during the quasi-static tests to gain insight in the response of these complex structures. Excellent agreement has been found between the quasi-static and impact test on the basis of the recorded contact force profiles.

I. Introduction

The high performance requirements of future aerospace transportation systems and the projected increased demand for air travel suggest the need for advanced and, perhaps, unconventional aerospace concepts. The Blended-Wing-Body (BWB), shown in Fig. 1, is an example of a revolutionary airplane concept that has potential for overall improvement in subsonic transport efficiency [1-5]. The improved performance of the BWB results from the blended configuration concept in which the fuselage centerbody (passenger cabin) and the wings are blended into a single lifting surface.

Based on finite element analysis, a set of critical design loads were developed for the most highly loaded central section fuselage cover panels (Fig. 1). The center-body cover panels must carry both the internal transverse pressure load, and the wing's bending and torsion loads. In particular, in a non-circular section the normal stresses due to internal pressure are noticeably higher than in a traditional narrow-body transport aircraft, which in turn leads to undesired increases to the weight of the structure. A variety of structural configurations for the pressurized cover panel structure were evaluated in a preliminary design study of the mega-transport BWB concept [1-3]. The configurations that were evaluated include conventional skin-stringer constructions with very deep hat-stiffeners, varying- and constant-depth sandwich structures, and separate structures for carrying the internal pressure and wing bending loads. On the basis of low weight, combined with ease of fabrication and assembly, a 5.5-inch-thick (140 mm) sandwich structure with graphite/epoxy facesheets and honeycomb core was chosen as the baseline cover panel structure concept. Core density and facesheet thickness vary as a function of local load, buckling, and deflection constraints.

¹Assistant Professor, Department of Aeronautics & Astronautics, University of Washington, Box 352400, Seattle, WA, 98195-2400 (USA). E-mail: feraboli@aa.washington.edu. Tel: 206.543.2170. Member AIAA.

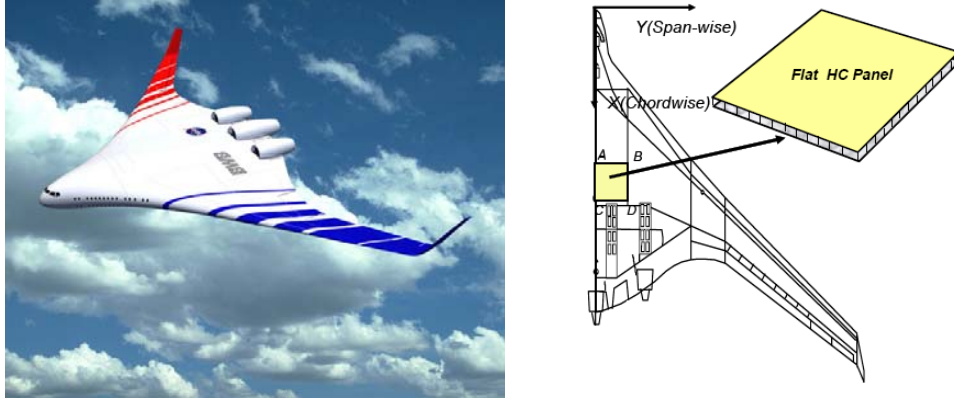


Fig. 1. BWB large commercial transport concept, and critically loaded crown panel with 5.5-inch-thick sandwich core [1].

The application of sandwich structures to primary aircraft structures has not reached its full potential, mostly because of their moisture absorption and retention characteristics, and because of an insufficient understanding of the impact-damage mechanisms and their effect on structural performance [6]. Foreign Object Damage (FOD) is the primary consideration for composite damage tolerance design and maintenance planning, since it can greatly reduce the stiffness and strength characteristics of composite laminated panels. FOD on sandwich structures can result in damage to the facesheets, the core, and the core-facesheet interface. Damage initiation thresholds, damage mechanisms, and damage extent depend on the properties of the facesheets and core materials, and on the interaction between the two.

Impact tests may be used to screen materials for damage resistance, in terms of the resulting damage size and mechanism, or in conjunction with a damage tolerance investigation, as in the case of Compression After Impact (CAI) testing [7-12]. In traditional low-velocity (drop tower) impact tests a composite target is subjected to a concentrated load by means of a falling weight, whose potential energy is specified. Subsequent damage tolerance studies use the projected damage area, dent depth and dent in-plane dimensions, or the very impact energy as the damage metric against which to plot residual performance [10-22]. With the advent of fully instrumented impact test devices, research has indicated that the recorded force-time histories can give greater insight in the dynamics of the event and mechanisms of damage. The use of an instrumented drop tower (e.g. Dynatup) enables the recording of the force-time history, with which it is possible to characterize the elastic behavior, failure initiation and failure propagation in terms of applied dynamic force and energy [19]. The greatest benefit in this type of test is the ability to identify the onset of failure in a composite structure. At sufficiently high impact energy levels, the contact force vs. time trace increases up to the point of failure, then a sudden drop occurs, which is followed by the onset of the low-frequency oscillations.

This investigation is aimed at developing a preliminary understanding of the damage resistance characteristics of these unique composite panels, via quasi-static and impact experiments, which will open the way to future, more extensive investigations. This investigation will also contribute to identifying the effect of facesheet thickness, core density, and core material on the transverse response and damage characteristics of the panels.

II. Previous Research

Various aspects of the low-speed impact response of sandwich panels have been addressed, at least in part, by previous research programs. These investigations have been conducted on honeycomb sandwich panels exhibiting core thicknesses of 0.375-0.75 inches (9.5-19 mm) and facesheets only a few plies thick, as those used for typical General Aviation [13-16]. In a few occasions, sandwich panels for candidate commercial transport aircraft [24, 25] were studied, which exhibited a maximum core thickness of 1.0 inch (25.4 mm), but facesheet thickness varying from 0.2 to 0.35 inches (5-8.9 mm). To the author's knowledge, characterization of the transverse response of

sandwich panels with thick core (> 3 inches or 76 mm) and relatively thick (0.110-0.220 inches or 2.8-5.6 mm) facesheets has not been conducted previously.

Hazizan and Cantwell [15] show that aluminum honeycomb cores are not strain-rate sensitive when loaded transversely by an indenter at velocities between 0.008 and 4.0 in/ min (0.2-102 mm/min). They also show that quasi-static indentation (QSI) tests can be used to calibrate simple energy balance models for predicting the impact response of sandwich panels.

Similarly, Tomblin et al. [13,14,16] employ QSI tests to obtain static load-deflection curves, and then insert them in Finite Element models for the prediction of the low velocity impact (LVI) response. The curves clearly exhibit a short initial elastic portion, usually of the order of half the facesheet thickness in depth, after which core crushing occurs. The onset of core damage is characterized by a substantial change in slope of the curve, which resembles the shape of a knee [26]. The load however continues to increase in the non-linear portion of the curve, which reaches a depth several times the facesheet thickness before the first skin fracture occurs. The onset of skin damage is characterized by a sequence of small drops in the load-deflection curve, which eventually lead to penetration and ultimate failure.

Tomblin and Raju [14] perform QSI tests on 0.375 and 0.75 in. (9.5 and 19 mm) thick cores, having relatively thin fabric facesheets, to determine the effect of skin and core thickness, as well as indenter size on the resulting damage state. It is found that increasing indenter size, increasing skin thickness, and decreasing core thickness has the effect of increasing the effective stiffness of the panel (higher force recorded for the same displacement). They suggest that the thinner core panels exhibit higher stiffness due to the higher buckling load of the shorter cell walls. Introducing a parameter called Energy Dissipation Factor (EDF), defined as the ratio of dissipated energy to maximum energy, they identify three regions associated with different failure mechanisms: core damage initiation, core damage propagation, and skin fracture. In particular, the second stage is associated to a nearly constant value of EDF. These are very similar to the regions identified in [27, 28] using the Coefficient Of Restitution (COR), defined as the square root of the ratio of the exit to incoming velocity.

Herup and Palazotto [29] conduct LVI and QSI tests on 0.5 in (12.7) thick Nomex honeycomb core panels having fabric skins with a thickness comprised between 4 and 48 plies. They observe the presence of a force threshold for damage initiation, which occurs at very low impact energy values, and is independent of the available kinetic energy of the falling weight. Similar conclusions were reported in [27] for solid laminated plates. They also observe that the ratio of absorbed to available energy is nearly constant after the onset of damage. Increasing skin thickness greatly increases the damage threshold, but at the same time increases the amount of energy absorbed in the creation of damage, hence the damage size. For thin facesheets, the contact force is transmitted directly from the impactor to the core, with very little chance of being dissipated and spread over a larger area. The onset of damage occurs earlier, the resulting core damage is greater and concentrated to a zone nearly the same size that of the impactor. For thicker facesheets, the laminate absorbs more energy in bending, and distributes the applied load over a greater area. Damage occurs at higher energy levels, but affects a greater portion of the core. It is also observed the threshold for facesheet fiber fracture also increases with skin thickness. The comparison between load-displacement curves for QSI and LVI test results are better for thin facesheets than for thick ones. Ultrasonic inspection reveals that the projected damage area for impact and static tests is the same if recorded at the same force level.

III. Materials and Experimental Setup

Eight sandwich configurations are considered to study the effect of facesheet thickness, core density and core material on their impact damage resistance. The sandwich panels (fig. 2A) are 20 in x 10 in x $(t_c + 2t_f)$ in., where t_c is the core thickness (5.50 in for aluminum and 5.25 in for the Nomex), and t_f is the facesheet laminate thickness (0.110, 0.165, and 0.220 inches). In SI units, 508 mm x 254 mm x $(t_c + 2t_f)$ mm, where $t_c = 140$ and 133 mm for the aluminum and Nomex respectively, and $t_f = 2.8, 4.2,$ and 5.6 mm.

The baseline core material is 5056 aluminum honeycomb, and three densities are considered for this investigation, namely 2.3, 3.1, and 3.8 pcf (lb/ft³), or 36.8, 49.6, and 60.9 kg/m³. A fourth, aramid (Nomex) honeycomb core alternative is also considered, having density of 4.0 pcf (64.1 kg/m³). The density is varied by changing cell size, not wall gage, which is kept constant. The facesheets are secondarily bonded to the honeycomb core using FM300 adhesive. A summary of all 8 configurations is reported in table I, while details on the core material properties are given in table II.

The composite facesheets are fabricated from AS4/3501-6 graphite-epoxy warp-knit preforms [30-33]. Each preform is a stack of material, which is equivalent to nine layers of unidirectional prepreg with 44%, 44% and 12% of 0, ± 45 , and 90 degree fibers, respectively, and therefore exhibits a bias in the 0 direction. The stacking sequence

has the form $[45/-45/0_2/90/0_2/-45/45]_{nT}$ with $n = 2, 3, 4$ for the three thickness values considered, and each stack has a cured thickness of 0.055 inches (1.44 mm). The dry preforms are arranged into stacks of the required thickness, and stitched with 0.125-in. (3.2 mm) step and 0.20 in (5.1 mm) spacing using Kevlar 29, 400-denier thread (the denier of a thread is the weight in grams of 9000 meters of that thread). The step regulates the amount of stitches per inch (SPI), in this case 8 (in reality between 7 and 9 stitches/inch), while the spacing is the distance between the rows of stitches. The stitching is aligned in the 0 fiber direction (fig. 2B). After stitching, the panels are impregnated with the epoxy resin using the Resin Film Infusion (RFI) process to make cured composite facesheets. The material properties for the stitched/RFI monolithic laminate are provided in [31], and reported in Table III.



Fig. 2 A, B. Sandwich panels used in the present investigation, having dimensions 20 in. x 10 in. x 5.5 in. (A), and close-up of the stitched CFRP skins (B).

Table I. Sandwich Panel Configurations.

Configuration ID	Facing Thickness in. [mm]	Core Material	Core Density lb/ft ³ [kg/m ³]	Core Thickness in. [mm]
AL1	0.165 [4.2]	Aluminum	3.1 [49.6]	5.50 [140]
AL2	0.165 [4.2]	Aluminum	2.3 [36.8]	5.50 [140]
AL3	0.165 [4.2]	Aluminum	3.8 [60.9]	5.50 [140]
AL4	0.220 [5.6]	Aluminum	3.1 [49.6]	5.50 [140]
AL5	0.220 [5.6]	Aluminum	3.8 [60.9]	5.50 [140]
AL6	0.110 [2.8]	Aluminum	3.1 [49.6]	5.50 [140]
AR7	0.165 [4.2]	Nomex	4.0 [64.1]	5.25 [133]
AR8	0.220 [5.6]	Nomex	4.0 [64.1]	5.25 [133]

Table II. Honeycomb core description and nominal properties.

Material	Cell size in. [mm]	Gage in. [mm]	Density lb/ft ³ [kg/m ³]
5056 AL	0.156 [4]	0.01 [0.25]	3.8 [60.9]
5056 AL	0.1875 [4.8]	0.01 [0.25]	3.1 [49.6]
5056 AL	0.25 [6.4]	0.01 [0.25]	2.3 [36.8]
HRH-10 AR	-	-	4.0 [64.1]

Table III. AS4/ 3501-6 facesheet description and elastic properties ($n = 2,3,4$).

Stacking sequence	E_x	E_y	G_{xy}	ν_{xy}
	Msi [GPa]	Msi [GPa]	Msi [GPa]	
$[45/-45/0_2/90/0_2/-45/45]_{nT}$	8.17 [56.3]	4.46 [30.7]	2.35 [16.2]	0.459

QSI and LVI tests are conducted on all panels using the same indenter/ impactor geometry and material, as well as boundary conditions. The panels are impacted at the panel center using a dropped-weight assembly, with an instrumented tup and a 1.0-inch-diameter steel tip (25.4 mm). In the initial LVI tests, the sandwich panels are clamped between two rigid rectangular support plates, with the impact area of the specimen centered over an unsupported aperture. Typical laminated and sandwich panels used in those investigation exhibit substantial deflection over the unsupported span, hence there is a need to identify the effect of boundary conditions on the effective structural stiffness, or the bending/ shear stiffness of the panel. The value of out-of-plane displacement of the back face is directly related to the support dimensions (aperture span), laminate thickness, and impactor dimensions. Furthermore, the displacement of the crosshead or falling weight is also a combination of the top face indentation (local), and back face panel deflection (global) [19]. For the panels considered in the present investigation, where the transverse dimension is of the same order of magnitude as the in-plane dimensions, and much greater than those of the impactor, the maximum deflection of the falling tup (including local indentation of the facesheet) in the initial LVI tests is less than 0.40 in. (10.2 mm), which is less than one-tenth of the overall panel thickness. After testing up to near-penetration energy levels, it is found that only a region of the core a few facesheet-thickness below the impacted (top) face is affected by damage, and that the bulk of the core's depth, as well as the back face, are not affected by damage occurring on the top facesheet. The top face is then identified to behave as a laminate supported on an elastic foundation. Subsequent LVI and QSI tests are then performed on the panels resting on a solid surface, without clamping or support fixtures.

LVI tests are carried out at energy levels of 10, 20, 30, and 50 ft lb (or 13.6, 27.11, 40.7, and 67.8 J), to impart different degrees of damage, ranging from barely visible (BVID) up to near penetration. A summary of all the tests performed on each panel configuration is given in table IV. After LVI testing, the specimens impacted at 30 ft lb (40.7 J) are subjected to measurement of the indentation depth by means of an automated depth gage machine. A contour plot of facesheet indentation depth is obtained, from which maximum in-plane dimension are easily determined. A selected number of specimens that were impact-damaged are also cross-sectioned, polished and inspected both visually and with the aid of a microscope to determine the extent of facesheet and core damage at different impact energy levels.

Table IV. QSI and LVI test matrix. The LVI column indicates impact energy (one per specimen tested), while QSI indicates the number of specimens tested.

Configuration	LVI ft lb [J]	QSI No. spec.
AL1	20, 30, 50 [27, 41, 68]	2
AL2	10, 20, 30 [14, 27, 41]	2
AL3	10, 20, 30, 50 [14, 27, 41, 68]	2
AL4	10, 30, 50 [14, 41, 68]	2
AL5	10, 30, 50 [14, 41, 68]	2
AL6	10, 20, 30 [14, 27, 41]	2
AR7	10, 30 [14, 41]	2
AR8	30 [41]	2

QSI tests are conducted up to maximum load (which may or may not involve penetration), and force-deflection curves are recorded. For a selected number of QSI tests, a three-dimensional digital imaging correlation technique is utilized to obtain full-field displacement measurements. The system, Vic-3D by Correlated Solutions Inc., consists of two high-resolution cameras and an image analysis computer program capable of measuring large displacements and strains [34]. The specimen is typically coated with a white spray paint, and a random pattern of black speckle marks is applied to the surface to be analyzed. The photogrammetry system captures images of the deforming object at predefined intervals during the test and compares them, thereby constructing a real-time plot of the deformation. These tests have been recently used in damage tolerance investigations, as CAI tests, where out-of-plane deformation is used to interpret the buckling behavior of damaged panels. In the present investigation, the three-dimensional imaging technique is used to monitor the out-of-plane deflection of the top facesheet during the QSI tests, and to investigate the possibility of adopting such method to obtain real-time indentation contours and profiles. To simplify the specimen preparation operation, a thin adhesive film is used that already contains a random distribution of black marks over a white background, and which is commercially available.

Quasi-static core compression/ crush tests are performed on 5 in. x 5 in. (127 mm x 127 mm) square panels by means of a flat steel platen in order to understand the honeycomb characteristics. All three aluminum honeycombs, as well as the Nomex, are tested, and core compression strength and crush strength are recorded.

IV. Results and Discussion

CORE COMPRESSION

After an initial nonlinear region, possibly due to the establishing of contact evenly across the facesheet, all specimens tested exhibit linear behavior. Failure manifests itself as a very sharp drop in the load-displacement curve (fig. 3), after which load picks up again at nearly half the value before failure. The load at failure is used in the literature to calculate the compressive strength of the core, stabilized because of the presence of the facesheets (see table V).

Of the four panels tested, one for each core density, the three aluminum (AL) cores exhibit very similar behavior. For the aluminum honeycomb, failure is preceded by the onset of elastic buckling waves along the length of the cells, which increase in number as the load is gradually increased, and release suddenly at the moment of failure (see fig. 4 A-C). In all three aluminum cores, failure is characterized by a zone of constant core crush right below the surface of the supported (not where the load is applied) skin. After failure, the load trace follows a short trough before assessing itself around a nearly constant value, associated to stable core crush propagation. This value is used in the literature to calculate the stabilized crush strength of the core. Both compressive and crush strengths are calculated as applied load over contact area.

The Nomex (AR) core exhibits a quite different behavior, as failure manifests in compression of the cells, followed by shifting and overlapping of the cell walls at the midplane of the panel (halfway from the facesheets). Furthermore, elastic buckling waves are not readily visible during the loading of the specimen, and after failure load follows a longer, more progressive trough. Eventually it reaches a near-asymptotic value, which in reality is a progressive linear increase at a very gradual rate.

Higher core density has the effect of increasing both the compressive (P_{co}) and crushing (P_{cr}) strengths of the aluminum core (figs. 3 and 5). From the limited data available, such increase in strength appears to be very similar for P_{co} and P_{cr} , with slightly greater benefits to the initial compressive strength (P_{co}) than to progressive crush strength (P_{cr}). With respect to the only Nomex core tested, it appears that compressive strength is quite lower than for equivalent-density aluminum cores, while crushing strength is hard to define as the load progressively increases rather than reaching a plateau as in the case of aluminum. However, if the portion of the load-deflection curve after the onset of core buckling is averaged, then the strength of the Nomex core is not very different from that of the aluminum core, see fig. 5.

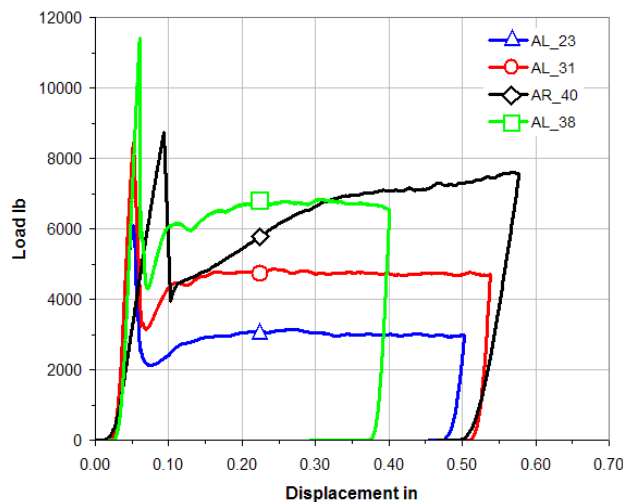


Fig. 3. Core compression and crushing curves.

Table V. Measured honeycomb stabilized compression and crush strengths.

Material	Measured Compr. Strength psi [MPa]	Typ.-Min. Compr. strength psi [MPa]	Measured Crush strength psi [MPa]	Nominal Crush strength psi [MPa]
5056 AL - 2.3 pcf	244.5 [1686]	265-155 [1827-1069]	120.9 [834]	100 [689]
5056 AL - 3.1 pcf	345.0 [2379]	410-260 [2827-1793]	187.8 [1295]	170 [1172]
5056 AL - 3.8 pcf	469.8 [3239]	500-375 [3447-2586]	278.0 [1917]	235 [1620]
HRH-10 AR - 4.0 pcf	361.2 [2490]	480-390 [3309-2689]	295.4 [2037]	-

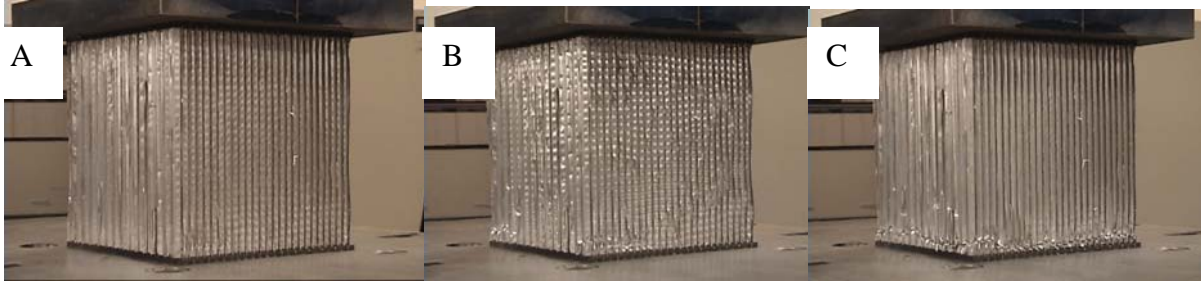


Fig. 4 A, B, C. Typical progression of honeycomb core compression test (panel AL6): during loading (A), immediately prior to failure (B), right after failure (C).

The elastic buckling of the honeycomb cell walls, which can be treated as buckling problem of a thin flat plate simply supported by the surrounding walls, yields [35]:

$$N_{cr} = k \frac{\pi^2 D}{b^2} \quad (1)$$

where D is the plate bending stiffness and b is the plate width. The critical load factor k is given by:

$$k = \frac{b^2}{a^2} \left(m + \frac{1}{m} \frac{a^2}{b^2} \right)^2 \quad (2)$$

where a is the length of the plate and m is an integer that corresponds to the number of half-waves along the length of the plate. It is known that for a/b ratios greater than 1, k becomes nearly independent of the aspect ratio itself, and assumes a value oscillating between value of 4 and 4.5. The m parameter tends asymptotically to the ratio a/b, and for the current core geometries and densities, the values of m are respectively 43, 36, and 26 for the 3.8, 3.1, and 2.3 pcf (60.9, 49.6, and 36.8 kg/m³) cores respectively. From fig. 4B it can be seen that the number of elastic buckling waves is indeed very close to 36 for panel AL6.

An observation that needs with regards to eq. 3 is that the elastic buckling load is independent of plate length for honeycomb cores whose height is greater than the cell size. Therefore the compression strength of honeycomb cores is independent of core height. The values supplied by the manufacturer for typical cores (0.625 in and 0.5 in height for metallic and non-metallic cores respectively, or 15.9 and 12.7 mm) are extendable to the ones of the present investigation. However, test results appear to fall between minimum and typical values, which is acceptable given that a statistically significant database could not be established.

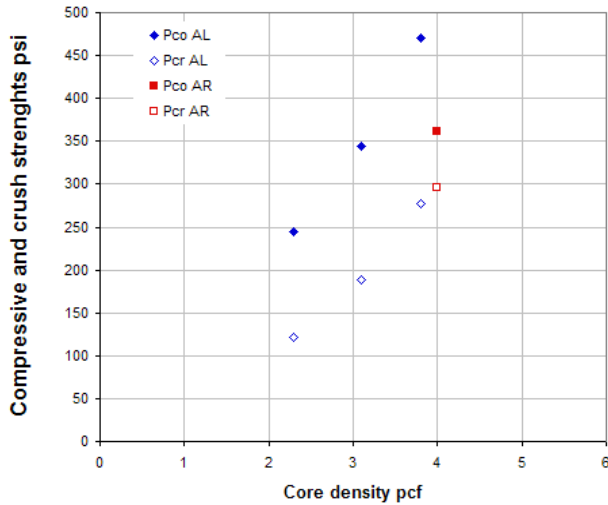


Fig. 5. Honeycomb core compression and crush strengths as a function of core density.

LOW-VELOCITY IMPACT

Specimens are tested at impact energy levels between 10 and 50 ft lb (13.6 and 67.8 J), which were deemed to be sufficient to create BVID and penetration respectively. Purely elastic test could not be achieved for these panels because the onset of core damage occurs at extremely low impact energy levels. At 10 ft lb (13.6 J) energy level, the force-time trace (fig. 6) exhibits a shape that differs from the sine wave typical of a purely elastic test, and resembles more a bell shape, typical of panels undergoing damage [27]. The trace corresponding to 10 ft lb (13.6 J) exhibits oscillations, which are difficult to interpret and at first analysis, could be attributed to either inertial response or the onset of damage. It will be shown in the following section that it is necessary to perform QSI tests in order to understand the actual behavior of the panel. Also visible on the 10 ft lb (13.6 J) trace, although not clearly, is a sharp jump in the force within the first 0.5 milliseconds, which again could be attributable to the inertial response of the specimen being displaced or to the transient response of the panel due to damage [23].

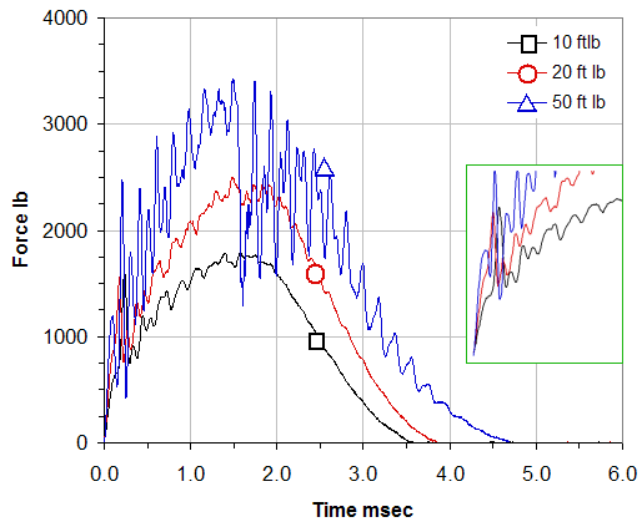


Fig. 6. Representative impact force-time traces (for specimen AL1) at increasing impact energy levels.

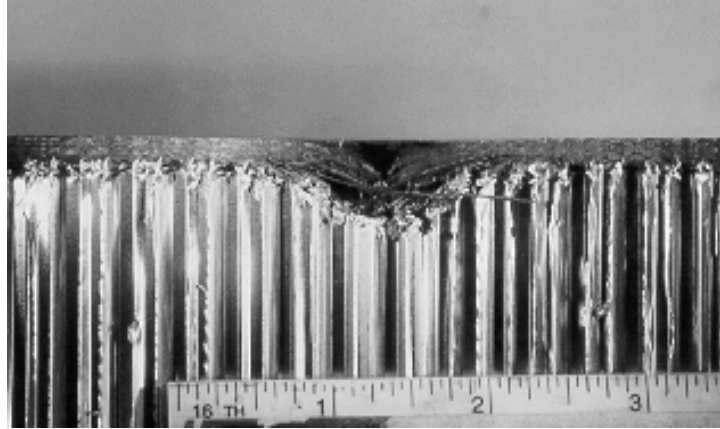


Fig. 7. Cross section of panel at the point of impact (50 ft lb) exhibits a very complex damage state. Core crushing is visible everywhere in the section immediately below the top facesheet, while fiber breakage and core-skin debonding is localized to the region below the impactor.

At 20 ft lb (27.1 J) of energy, the force-time trace reaches a higher peak value (fig. 6), the initial spike is slightly more pronounced, and the overall contact duration is noticeably greater, thereby confirming that greater damage has been introduced in the panel, although still barely visible.

At 50 ft lb (67.8 J) impact energy, the initial spike is much more pronounced and a series of other spikes characterize the signal, thereby suggesting the creation of extensive damage. The observation is confirmed by the even greater duration of the contact event [27]. Furthermore, toward the peak there is a sharp drop in the force, also followed by low frequency oscillations, which indicates the onset of through-laminate fiber breakage.

After cross sectioning, the specimens reveal a localized area of extensive skin laminate damage, comprising delaminations and fiber breakage, as well as disbonding of the core from the facesheet. The latter is attributable to the fact that the aluminum core, which has undergone plastic deformation, does not recover its original shape to the same extent of the composite skin. However, it is very interesting to observe that a very large area of core cell buckling, 6-8 times the diameter of the impactor, affects the immediately below the top skin, for an average depth of up to half the laminate thickness (fig. 7).

The specimens that were impacted at 30 ft lb (40.7 J) are subjected to indentation depth measurement by means of automated depth gage machine, from which contour plots can be obtained, see fig. 8 A, B. It can be seen that there is a limited, nearly circular area of greater dent depth close to the impact site, and a much larger but shallower area, elliptical in shape, which can reach in-plane dimensions several times those of the impactor. The elliptical shape of the larger indentation is due to the anisotropic elastic properties of the facesheets, which exhibit a bias in the longitudinal modulus. Plotting the depth of indentation along the major and minor axes of the ellipse yield the distribution of fig. 9.

Results are reported in table VI, and show that for increasing facesheet thickness and decreasing core density the area becomes larger but more shallow, while for thinner skins and heavier cores it becomes more concentrated but of greater depth. The thicker, hence stiffer, skins are thought to provide greater resistance to penetration, and hence to distribute the load to a greater area across the core. On the other hand, the thin skins are more prone to localized fracture damage, and hence concentrate the energy and load to a smaller area below the impactor. It has to be observed that while facesheet thickness greatly affects dent depth and depression size, core density has only a secondary effect, particularly on dent depth. The consequences of these observations on the damage tolerance characteristics are not yet known, as a shallower but larger region of skin curvature may reduce the compressive strength of the crown panel more than a deeper but concentrated area. In general the effects of varying facesheet thickness on dent size (length of major and minor axes) are much more pronounced than those of core density, and even more so for dent depth, which is very sensitive to skin thickness but nearly independent of core density [6].

A last consideration needs to be made with regards to the Nomex core, which exhibits in general much shallower and smaller indentation contours, phenomenon which is attributable to the spring back characteristics of the material, which recovers its shape much more than aluminum after buckling.

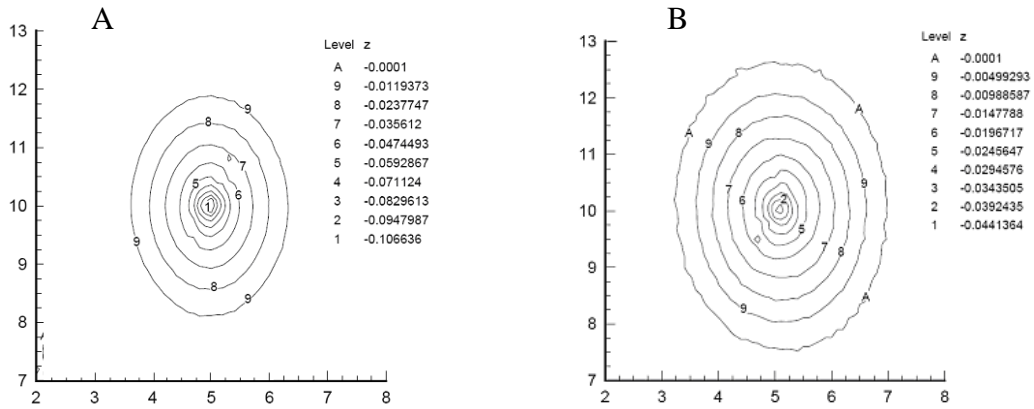


Fig. 7 A, B. Representative indentation depth contours for configurations AL6 (A) and AL2 (B) at 30 ft lb.

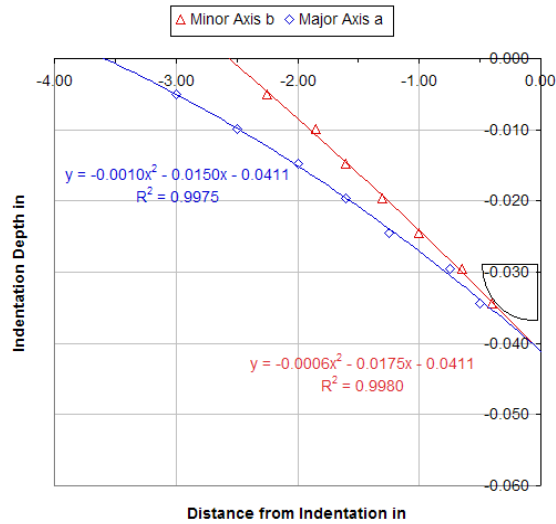


Fig. 9. Indentation profiles through the thickness along the two axes of the elliptical indentation (impactor shown in scale at midplane).

Table VI. Indentation depth and in-plane dimensions for 30 ft lb impacts on all configurations.

Test	Max indentation depth in	Max. measured indentation axis (long) in	Max. measured indentation axis (short) in
AL1 I30	0.044	5.10	3.75
AL2 I30	0.044	5.45	4.25
AL3 I30	0.041	4.50	3.25
AL4 I30	0.035	>6.00	>5.00
AL5 I30	0.034	4.00	3.15
AL6 I30	0.106	3.75	2.65
AL7 I30	0.014	1.90	1.45
AL8 I30	0.099	1.75	1.05

PREDICTION OF INDENTATION SIZE

The elastic response of sandwich panels due to the application of a point force can be separated into a symmetric and an anti-symmetric mode, due to indentation and bending respectively [36, 37]. The total deflection of the plate is then the sum of the individual deflections. Since the transverse dimensions of the panels used in this investigation is of the same order of magnitude of the in-plane dimensions, and large compared to the impactor dimensions, bending of the back facesheet can be neglected. The top facesheet therefore can be accurately modeled as a plate on elastic foundation [36, 37], and the panel's deformation behavior can be reduced to the indentation response of the top facesheet over the core. The elastic indentation of a large anisotropic sandwich panel subjected to a point load is associated to the equivalent spring constant of length t_c , given by $\beta = 2E_{zz}/t_c$ [37], where E_{zz} is the flat-wise modulus of the core, and the $t_c/2$ represents half of the core thickness, as this value corresponds to the symmetric mode of deformation.

The influence zone, or the area experiencing elastic deformation, for a point force is confined to a circular zone with a maximum diameter determined by [37]:

$$d_{\max}^{el} = 7.8 \left(\frac{D_f t_c}{2E_{zz}} \right)^{\frac{1}{4}} \quad (3)$$

where D_f is the bending stiffness of an isotropic facesheet. In case of orthotropic facesheets, D_f can be substituted by the value of D_{avg} , which is the in-plane average bending stiffness, defined as $D_{avg} = \sqrt{D_{11} D_{22}}$.

Alternatively, the value of D_f can be replaced by D_{11} or D_{22} for improved accuracy, in which case eq. 3 gives the values of the maximum and minimum axes of an ellipse, elongated in the direction of greater bending stiffness. The maximum diameter of influence as determined by eq. 3 is valid only for the elastic indentation of the core, hence for impact events that don't introduce permanent core indentation and damage.

In case of severe impacts Lin [37] recommends the problem to be viewed as a facesheet sitting on an elastic foundation of half the spring constant $\beta = E_{zz}/t_c$. The resulting zone of influence, which is the core crush zone, therefore becomes:

$$d_{\max}^{dmg} = 7.8 \left(\frac{D_f t_c}{E_{zz}} \right)^{\frac{1}{4}} \quad (4)$$

which is 1.68 times smaller than the maximum elastic diameter given by eq. 3. The maximum crush zone diameter is therefore related only to the facesheet bending stiffness (skin thickness, modulus and Poisson's ratio). If the average modulus E_{avg} is used, an average circular indentation is obtained, while if the actual E_{11} or E_{22} values are used an elliptical dent is obtained. The results of eq. 4 applied to the eight configurations tested are reported in table VII and it is seen that they tend to somewhat overestimate by a few percent the measured values reported in table VI. However, it has to be noted that the test data was collected only for 30 ft lb (40.7 J) impacts, which may not be sufficient to generate the maximum indentation achievable. Further investigation needs to be performed, but it

appears that eq. 4 can yield relatively accurate estimates of dent size for the 1.0-in. (25.4 mm) diameter indenter even though it makes the assumption of point force application.

Table VII. Maximum indentation dimensions as predicted by eq. 4 for the Aluminum core.

Configuration	Max. predicted indentation axis (long – E_{11}) in	Max. predicted indentation axis (short – E_{22}) in
AL1	5.34	4.60
AL2	6.08	5.22
AL3	4.88	4.18
AL4	6.62	5.70
AL5	6.04	5.20
AL6	3.94	3.38

QUASI-STATIC INDENTATION

It has been previously shown that before exploring the impact characteristics of composite panels it is highly beneficial to perform an identical test under quasi-static conditions [23, 27, 28]. It is however important to employ the identical impactor/fixture/target assembly. In the present investigation, the specimens, resting on a rigid surface, are indented at the center of the top skin using the same indenter material and size as in the LVI tests.

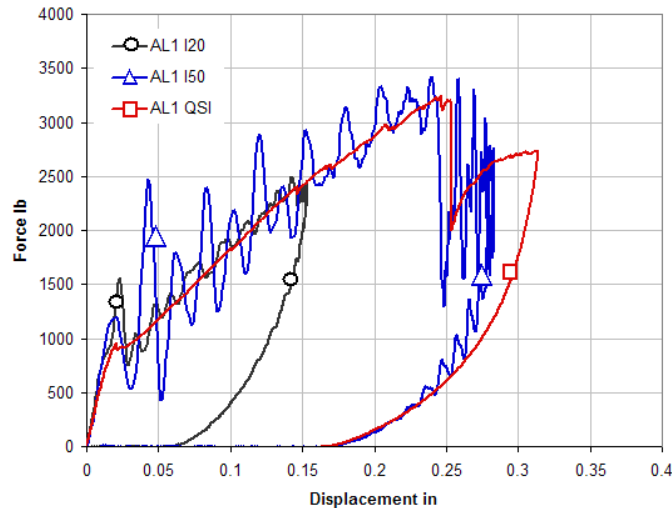


Fig. 10. QSI load-displacement curve for configuration AL1, and superimposed impact traces at two impact energy levels (20 and 50 ft lb).

The derivation of impact force-displacement curves from available force-time data allows for an immediate comparison with the results obtained from a QSI test, and it is generally accepted in the literature that, for current polymer composite systems, QSI and LVI traces superimpose well [17-21, 23, 27, 28]. Furthermore, the values for the onset of damage and the maximum force reachable during an impact test have also been found to be very close, often coinciding with the mean static failure and ultimate loads [27]. That is indeed the case for the panels in this investigation, where load-deflection curves superimpose well for all configurations tested (fig. 10).

Perhaps the most important result of performing QSI tests is that they make readily observable the presence of a “knee” in the load-deflection curve, occurring at very low values of applied load, which indicates the onset of damage [14]. This behavior was not readily observable in the impact traces of fig. 6, as it is easily masked by the presence of other vibratory phenomena. The importance of performing QSI tests is readily observable in fig. 10 where, beside the mentioned knee, a series of secondary failures before ultimate load can be easily detected on the QSI curve, but not in the LVI trace.

The other important use of a preliminary QSI test is that from integration of the load-displacement data, it is possible to obtain the values of the static deformation energy, and to build a force-energy curve [23, 27, 28]. For strain-rate insensitive materials, such as contemporary carbon/epoxy systems, the quasi-static force-energy curve, virtually coincides with the impact maximum force-energy, and is an excellent tool to predict the force generated at various impact energy levels [23]. The curves shown in figs. 11 A, B for three configurations are a clear example of how the QSI force-energy curves can be used to estimate maximum impact forces for discrete values of impact energy. The quasi-static nature of low-velocity impact events is such that it allows the translation of indentation tests data into impact data with more than acceptable accuracy.

The curve indicates that for configuration AL4 the onset of core crushing occurs at impact energy levels between 1.0 and 1.5 ft lb (1.36-2.03 J), and for panels AL1 and AL6 at less than 1.0 ft lb (1.36 J). These observations would have been particularly hard to be made with drop tower setups, where the impactor assembly, usually weighing at least 1.5 lb (0.68 kg), would require drop heights of only a few inches in order to highlight this threshold. Lastly, the curve shows that for panel AL4, ultimate load is reached at around 65-70 ft lb (88.1-94.9 J) impact energy, and for panel AL1 at around 35 ft lb (47.5 J). Although testing at impact energy levels greater than those required to achieve ultimate load will not result in greater contact forces or indentation sizes, it will yield increasing amounts of core and facesheet impact damage [23,27].

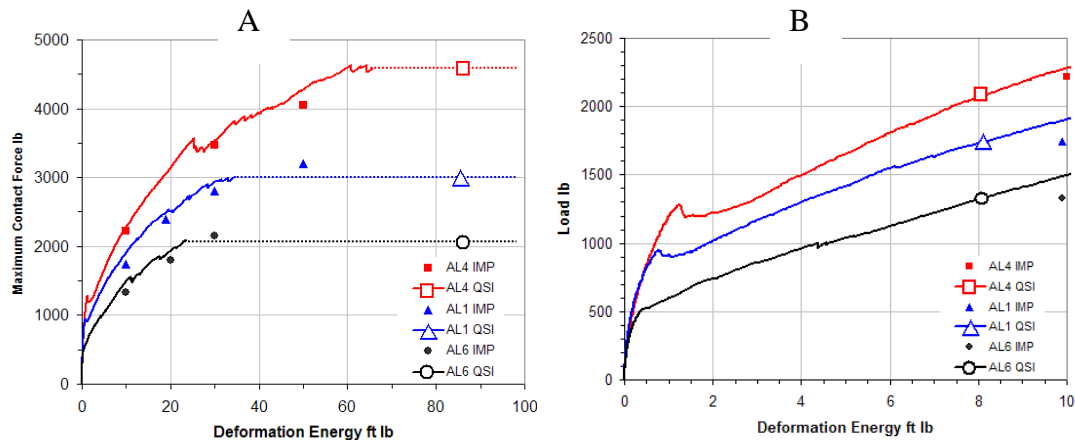


Fig. 11 A, B. A) QSI Load-Energy curves for three configurations, and juxtaposed maximum impact force values for discrete impact energy levels. B) Close-up on initial region of the curves.

The QSI investigation, in support of the LVI tests, is particularly suitable for comparing the behavior of the eight structural configurations considered. The effect of varying skin thickness, for the same core density, has great effects on the overall shape of the LD curve, as shown in fig. 12A. The thicker facesheets appear also to exhibit more secondary drops in the LD curve due to laminate damage accumulation. It can be seen how the first failure load (P_1), due to onset of core crushing, increases notably with skin thickness, as does the ultimate failure load (P_{max}). These trends are reported in fig. 12B for all panels tested (where it was possible to compare configurations). The effect of varying core density, for the same skin thickness, appears to have a much smaller effect on the general shape of the LD curve, as shown in fig. 13A. The first failure load (P_1), due to onset of core crushing, is nearly insensitive to core density, for the three panels with aluminum core, and so appears to be the ultimate failure load (P_{max}). Core density seems to affect only the slope of the LD curve after the onset of core crushing, which is lower for lower density

cores. Therefore core density appears to affect the stiffness of the panel but only in the post-elastic regime, suggesting that the denser cores retain greater stiffness and therefore provide greater support to the facesheets. These trends are even more evident in fig. 134B for all panels tested (where it was possible to compare configurations). Note that the 4.0 pcf (64.1 kg/m³) core density belongs to the Nomex honeycomb, which explains the difference in P₁ and P_{max} trends, as well as the difference in the slope of the LD curve.

It appears therefore that for the limited number of cores and skins considered in this investigation, skin thickness has a primary effect on the damage resistance characteristics of the panel, while core density (varied by varying cell size, not cell gage) appears to have a secondary effect. This observation is in direct contrast with the results obtained from quasi-static compression (not indentation) of the core, which show great differences in compression and crushing strength. This difference could be attributable to the localized nature of the indentation response, but further work is required to understand the problem.

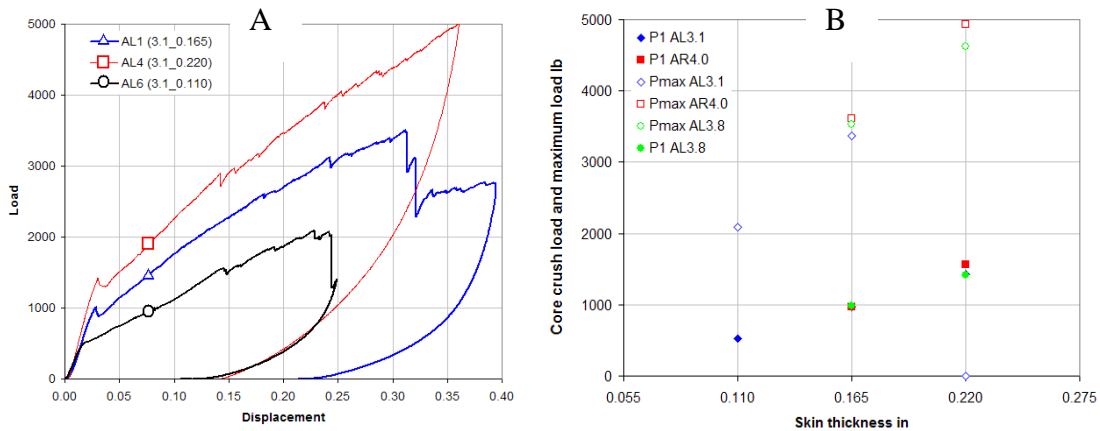


Fig. 12 A, B. A) Effect of skin thickness (same core density) on load-displacement curves for three configurations. B) General trends observed for first and ultimate failure loads for various configurations tested.

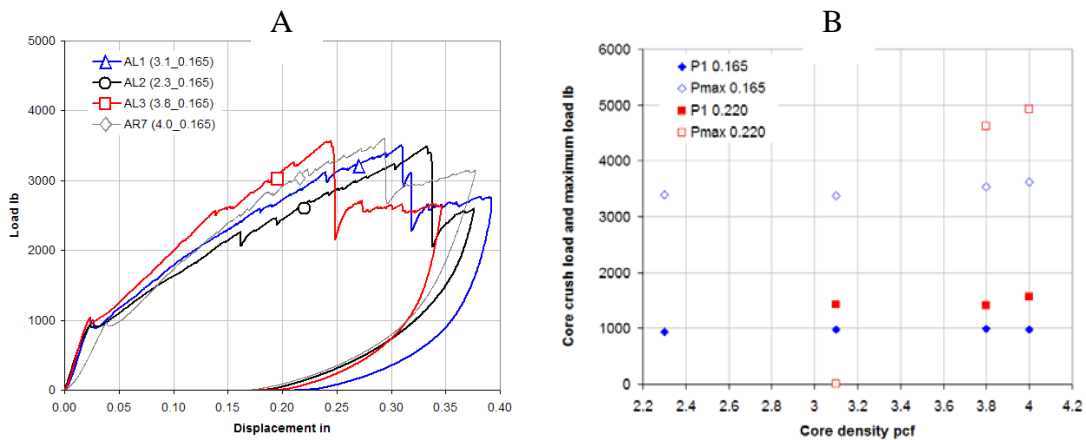


Fig. 13 A, B. A) Effect of core density (same skin thickness) on load-displacement curves for four configurations. B) General trends observed for first and ultimate failure loads for various configurations tested.

A further observation in support of the difference between compression and indentation results can be found, although indirectly, in Raju and Tomblin [14]. Their investigation featured QSI of two core thicknesses, 9.525 mm and 0.75 in. (19.05 mm), having a cell size of 0.1875 in. (4.7625 mm). They performed QSI tests and reported notable differences in the first and ultimate failure loads. This result is in contrast with core compression and crush test results, which are known to be independent of core thickness (see section above). It appears that static indentation and compression, although they both create failure by local plastic buckling of the cell walls, they also involve very different deformation phenomena, which justify the sensitivity to different parameters. Caution needs then to be used when selecting core material for damage resistance based upon compression strength data available from the supplier.

Three additional specimens were tested for QSI in conjunction with the 3D imaging correlation technique. The system was successfully used to monitor real-time development of the depression/ indentation, and typical contours of the elliptical depression, shown in fig. 14, are consistent with depth-gage measurements. Unfortunately, the presence of the indenter prevents the monitoring of the dent size evolution underneath the indenter, which blocks the vision field of the two cameras. Although the use of this technique did not highlight instabilities or other particular phenomena during the progress of the crush, it did allow for visualizing the evolution of the dent, thereby supporting the indentation measurements obtained by the depth gage.

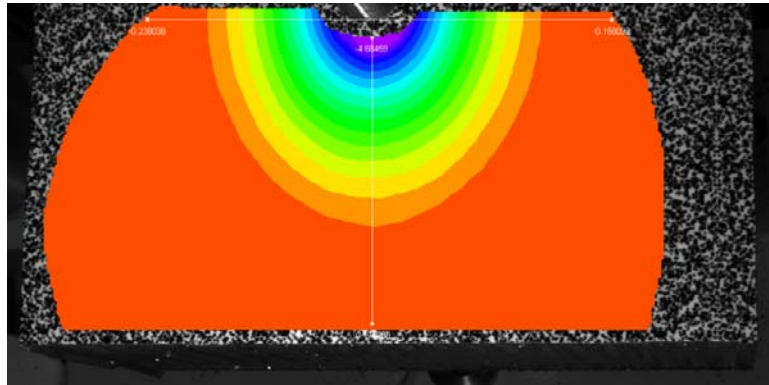


Fig. 14. Real-time transverse displacement (indentation) contour obtained by 3D digital imaging correlation.

V. Conclusions

The investigation has shown that thick-honeycomb-core panels are particularly susceptible to FOD, as introduced by means of quasi-static indentation or low-velocity impact. The onset of core crushing occurs at very low values of impact energy or contact force, and the threshold is hard to detect in the impact force-time histories. This goes in further support of previous recommendations of always performing QSI tests before evaluating impact test data.

Core crushing is associated to a permanent depression of the impacted specimen, exhibiting a large, shallow elliptical shape, and an area of greater depth localized underneath the impactor. A simple formula previously suggested by Lin for the prediction of the maximum indentation dimensions has revealed to be particularly accurate for the panels tested. Stitching could have a detrimental effect because by preventing extensive delamination from occurring in the facesheets tends to concentrate the energy in the deformation of the core.

It has been found that for the range of skin thicknesses and core densities evaluated, skin thickness has a primary effect on the damage resistance characteristics of the panel, while core density (varied by varying cell size, not cell gage) appears to have a secondary effect. This observation is in direct contrast with the results obtained from compression/ crushing (not indentation) of the core, which show great differences in strength. In general, core compression/ crushing strength is not a suitable indicator of the damage resistance behavior of these sandwich panels.

References

- ¹Liebeck, R. H., Page, M. A., Rawdon, B. K., "Blended-Wing-Body Subsonic Commercial Transport", 36th AIAA Aerospace Sciences Meeting and Exhibit, Reno, NV, No. 98-0438, January 1998.
- ²Liebeck, R. H., "Design of the Blended Wing Body Subsonic Transport", *Journal of Aircraft*, Vol. 41, No. 1, January-February 2004, pp. 10-25.
- ³Potsdam, M. A., Page, M. A., Liebeck, R. H., "Blended-Wing-Body Analysis and Design", 38th AIAA Structures, Structural Dynamics and Materials Conference, Atlanta, GA, No. 97-2317, April 1997.
- ⁴Mukhopadhyay, V., "Blended Wing Body (BWB) Fuselage Structural Design for Weight Reduction", 46th AIAA Structures, Structural Dynamics and Materials Conference, Austin, TX, No. 2005-2349, April 2005.
- ⁵Mukhopadhyay, V., Sobieszczanski-Sobieski, J., Kosaka, I., Quinn, G., Vanderplaats, G. N., "Analysis, Design and Optimization of Non-cylindrical Fuselage for Blended-Wing-Body Vehicle", *Journal of Aircraft*, Vol. 41, No. 4, July-August 2004, pp. 925-930.
- ⁶Ilcewicz, L.B., Smith, P.J., Hanson, C.T., Walker, T.H., Metschan, S.L., Mabson, G.E., Willden, K.S., Flynn, B.W., Scholz, D.B., Polland, D.R., Fredrikson, H.G., Olson, J.T., Backman, B.F., "Advanced Technology Composite Fuselage - Program Overview" NASA CR4734, April 1997.
- ⁷Razi, H., Ward, S., "Principles for achieving damage tolerant primary composite aircraft structures", DoD/FAA/NASA 11th Conference on Fibrous Composites in Structural Design, Aug. 1996.
- ⁸MIL-HDBK-17, Handbook on Composite Materials, Rev. 3F, Ch. 7, Durability, Damage Resistance, and Damage Tolerance, Material Science Corp., 2002.
- ⁹National Materials Advisory Board, "New Materials for Next Generation Commercial Transports", National Research Council, NMAB-476, National Academy Press, 1996.
- ¹⁰Kan, H.P., "Enhanced reliability prediction methodology for impact damaged composite structures", DOT/FAA/AR-97/79, Oct. 1998.
- ¹¹Kan, H.P., Mahler, M., "Effects of stiffener/rib separation on damage growth and residual strength", DOT/FAA/AR-95/12, May 1996.
- ¹²Kan H.P., Graves, M.J., Horton, R.E., Whitehead, R.S., et al., "Damage Tolerance of Composites, Vol. III: Analysis, Methods, Development, and Test Verification", Air Force Wright Aeronautical Laboratories, AFWAL-TR-87-3030, July 1988.
- ¹³Tomblin, J. S., Raju, K. S., Arosteguy, G., "Damage resistance and tolerance of composite sandwich panels - scaling effects", DOT/FAA/AR-03/75, February 2004.
- ¹⁴Tomblin, J. S., Raju, K. S., "Damage characteristics in sandwich panels subjected to static indentation using spherical indentors", 42nd AIAA Structures, Structural Dynamics, and Materials Conference, Seattle, WA, Paper 2001-1189, April 2001.
- ¹⁵Hazizan, M.A., Cantwell, W.J., "The low velocity impact response of an aluminum honeycomb sandwich structure", *Composite Part B: Engineering*, 34, 2003, pp. 679-687.
- ¹⁶Tomblin, J. S., Raju, K. S., Liew, J., Smith, B.L., "Impact damage characterization and damage tolerance of composite sandwich airframe structures", DOT/FAA AR-00/44, January 2001.
- ¹⁷Jackson, W. C., Portanova, M. A., "Out-of-Plane Properties", Mechanics of Textile Composites Conference, NASA CP 3311, Part 2, pp. 315-348, October 1995.
- ¹⁸Portanova, M. A., "Impact Testing of Textile Composite Materials", Mechanics of Textile Composites Conference, NASA CP 3311, Part 2, pp. 391-423, October 1995.
- ¹⁹Jackson, W. C., Poe, C. C. Jr., "The use of Impact Force as a Scale Parameter for the Impact Response of Composite Laminates", *Journal of Composites Technology and Research*, Vol. 15, No. 4, Winter 1993, pp. 282-289.
- ²⁰Poe, C. C. Jr., Harris, C. E., "Mechanics methodology for textile perform composite materials", Sixth NASA/DoD Advanced Composites Technology Conference, NASA CP 3326 Part 1, pp. 95-130, June 1996.
- ²¹Poe, C. C. Jr., Portanova, M. A., Masters, J. E., Sankar, B. V., Jackson, W. C., "Comparison of Impact Results for several Polymeric Composites over a wide range of impact velocities", First NASA/DoD Advanced Composites Technology Conference, NASA CP 3104 Part 2, pp. 513-547, January 1991.
- ²²Nettles, A. T., Douglas, M. J., Estes, E. E., "Scaling Effects in Carbon/Epoxy Laminates Under Transverse Quasi-Static Loading" NASA TM 209103, March 1999.
- ²³Feraboli, P., "Some recommendations for the characterization of the impact performance of composite panels by means of drop tower impact testing", *Journal of Aircraft*, AIAA, in press 2006.
- ²⁴McGowan, D. M., Ambur, D. R., "Damage-Tolerance Characteristics of Composite Fuselage Sandwich Structures with Thick Facesheets", NASA TM 110303, February 1997.

- ²⁵McGowan, D. M., Ambur, D.R., "Compression Response of a Sandwich Fuselage Keel Panel With and Without Damage", NASA TM 110302, February 1997.
- ²⁶Koissin, V., Shipsha, A., Rizov, V., The inelastic quasi-static response of sandwich structures to local loading, *Composite Structures* 64, 2004, pp. 129-138.
- ²⁷Feraboli, P., Kedward, K. T., "Enhanced Evaluation of the Low-Velocity Impact Response of Composite Plates", *AIAA Journal*, 42/10, October 2004, pp. 2143-2152.
- ²⁸Ambur, D. R., Prasad, C. B., Rose, C. A., Feraboli, P., Jackson, W. C., "Scaling the Non-linear Impact Response of Flat and Curved Composite Panels", 46th AIAA Structures, Structural Dynamics and Materials Conference, Austin, TX, No. 2005-2224, April 2005.
- ²⁹Herup, E.J., Palazotto, A.N., "Low velocity impact damage initiation in graphite/epoxy/nomex honeycomb sandwich plates", *Composites Science and Technology*, 57, 1997, pp. 1581-1598.
- ³⁰Hinrichs, S., Chen, V., Jegley, D., Dickinson, L. C., Kedward, K., "Effect of Impact on Stitched/RFI Compression Panels", Fifth NASA/ DoD Advanced Composites Technology Conference, NASA CP 3294 Vol. I Part 2, pp. 879-912, May 1995.
- ³¹Wang, J. T., Jegley, D. C., Bush, D. C., Hinrichs, D. C., "Correlation of Structural Analysis and Test Results for the McDonnell Douglas Stitched/RFI All-Composite Wing Stub Box", NASA TM 110267, July 1996.
- ³²Jegley, D. C., Bush, H. G., Lovejoy, A. E., "Structural Response and Failure of a Full-scale Stitched Graphite-Epoxy Wing", 42nd AIAA Structures, Structural Dynamics and Materials Conference, Seattle, WA, No. 2001-1334, April 2001.
- ³³Markus, A. M., Grossheim, B. G., "Manufacturing Development for Stitched/RFI Transport Wing Stub Box Structures", Fifth NASA/ DoD Advanced Composites Technology Conference, NASA CP 3294 Vol. I Part 2, pp. 773-786, May 1995.
- ³⁴McGowan, D. M., Ambur, D. R., Hanna, T. G., McNeill, S. R., "Evaluation of the Compressive Response of Notched Composite Panels Using a Full-Field Displacement Measurement System", 40th AIAA Structures, Structural Dynamics and Materials Conference, St. Louis, MO, No. 99-1406, April 1999.
- ³⁵Timoshenko, S., Woinowsky-Krieger, S., "Theory of plates and shells", 2nd ed., McGraw-Hill, New York, 1959.
- ³⁶Olsson, R., McManus, H.L., "Improved theory for contact indentation of sandwich panels", *AIAA Journal*, 34/6, June 1996, pp. 1238-1244.
- ³⁷Lin, W., "The point force response of sandwich panels and its application to impact problems", 37th AIAA Structures, Structural Dynamics and Materials Conference, Reston, VA, No. A926884, April 1996.